Matter and Radiation at Extremes | LETTER | scitation.org/journal/mre

XFEL and HHG interaction with matter: Effects of ultrashort pulses and random spikes

Cite as: Matter Radiat. Extremes 6, 034001 (2021); doi: 10.1063/5.0046040
Submitted: 31 January 2021 • Accepted: 25 February 2021 •
Published Online: 29 March 2021

F. B. Rosmej,[1,2,3,4,a)] V. A. Astapenko,[3] and E. S. Khramov[3,b)]

AFFILIATIONS

[1]Sorbonne University, Faculty of Science and Engineering, UMR 7605, Case 128, 4 Place Jussieu, F-75252 Paris Cedex 05, France
[2]LULI, Ecole Polytechnique, CEA, CNRS, Laboratoire pour l'Utilisation des Lasers Intenses, Physique Atomique dans les Plasmas Denses, F-91128 Palaiseau, France
[3]Moscow Institute of Physics and Technology—MIPT, Institutskii per. 9, Dolgoprudnyi 141700, Russia
[4]National Research Nuclear University MEPhI (Moscow Engineering Physics Institute), Kashirskoe sh. 31, Moscow 115409, Russia

[a)]**Author to whom correspondence should be addressed:** frank.rosmej@sorbonne-universite.fr
[b)]egor.khramov@phystech.edu

ABSTRACT

The theory of photoionization describing the interaction of x-ray free-electron laser (XFEL) pulses and high-harmonic-generated (HHG) radiation is generalized to ultrashort laser pulses, where the concept of the standard ionization probability per unit time in Fermi's golden rule and in Einstein's theory breaks down. Numerical calculations carried out in terms of a generalized photoionization probability for the total duration of pulses in the near-threshold regime demonstrate essentially nonlinear behavior, while absolute values may change by orders of magnitude for typical XFEL and HHG pulses. XFEL self-amplified spontaneous emission pulses are analyzed to reveal general features of photoionization for random and regular spikes: the dependences of the nonlinear photoionization probability on carrier frequency and spike duration are very similar, allowing an analytical expectation value approach that is valid even when there is only limited knowledge of random and regular parameters. Numerical simulations carried out for typical parameters demonstrate excellent agreement.

Plasma physics is concerned with the properties of a statistical system containing many charged particles and in which long-range Coulomb forces play an important role in establishing collective phenomena. As the density is increased and the temperature lowered, the plasma begins to exhibit features characteristic of condensed matter, where short-range as well as long-range forces are important. In this regime, the so-called "strongly coupled many-particle Coulomb system," quantum statistics, dynamic effects, and the interplay between atomic, molecular, and nuclear physics become major issues.[1,2] Associated with these properties is the emergence of features such as insulator-to-metal transitions, order–disorder transitions, and chemical separation. The microscopic properties of these plasmas depend on phase transitions, which in turn affect the macroscopic properties of the plasma through the rates of elementary and transport processes.

With the rapid development of powerful laser installations, high-energy-density laser-produced plasmas, strongly coupled plasmas, and warm dense matter (matter near solid density, with temperatures of the order of the Fermi energy) have become major areas of research in high-energy-density physics, relevant to a wide range of topics:[3–10] dense-plasma astrophysics; the interiors of white and brown dwarfs, the Sun, neutron stars, and giant planets; dense laboratory plasmas (including metals, alloys, and semiconductors); and a variety of plasmas produced by diamond-anvil cells, metal vaporization, shock compression, and pinches. Dense strongly coupled plasmas and warm dense matter are exotic conditions of matter that are extremely challenging to investigate, and there is a great need for experimental studies to advance the subject. In many cases, x-ray emission from the sample under study itself provides a unique characterization: opacity is low, allowing recordings of volumetric self-emission of the sample. However, the matter of interest here (strongly coupled plasmas and warm dense matter) typically has a temperature of the order of the Fermi energy (the order of 10 eV). Target self-emission in the x-ray range is therefore negligible.

To circumvent the absence of volumetric x-ray self-emission, essentially two methods have been developed. One of these employs

high-intensity lasers: the interaction with the near-solid-density matter generates suprathermal electrons that in turn ionize inner atomic shells of the "warm" target material, with the subsequently emitted radiation being in the x-ray spectral range.[11–13] For example, for K-shell ionization of partially ionized copper and the corresponding x-ray K_α emission, we have

$$K^2L^8M^x + e_{\rm hot} \rightarrow K^1L^8M^x + 2e \rightarrow K^2L^7M^x + 2e + \hbar\omega_{K_\alpha}, \quad (1)$$

where the electronic configurations are described by the number of electrons (upper index) present in given shells (K, L, M), x indicates the degree of ionization of the heated sample (e.g., $x = 18$ for singly ionized copper, $x = 17$ for doubly ionized copper, ...), $e_{\rm hot}$ is an electron with "suprathermal" energy, and ω_{K_α} is the frequency of the K_{alpha} transition. The other method is similar, but instead of suprathermal electrons, a pulse from an x-ray free-electron laser (XFEL)[14–17] is used:

$$K^2L^8M^x + \hbar\omega_{\rm XFEL} \rightarrow K^1L^8M^x + e_{\rm photo}, \quad (2)$$

where $\omega_{\rm XFEL}$ is the frequency of the XFEL photons and $e_{\rm photo}$ is a photoionized electron. The tuning capabilities of XFELs (in particular with regard to frequency and pulse duration) make them exceptional tools for fundamental studies.[9,10]

According to standard quantum mechanical perturbation theory, the total probability W of a transition during an electromagnetic pulse is equal to the probability per unit time w multiplied by the pulse duration τ. The probability W corresponds to Fermi's famous golden rule that connects the total probability with the probability per unit time via the cross-section of the photo-process $\sigma_{\rm photo}$ and the photon flux density $j_{\rm ph}$ according to $w = W/\tau \propto \sigma_{\rm photo} j_{\rm ph}$. This relation corresponds to Einstein's theory of stimulated emission and absorption: the number of photon absorptions per unit time $N_{\rm abs}$ is described by the Einstein coefficient of stimulated absorption $B_{\rm abs}$, i.e., $N_{\rm abs} = N_{\rm low} B_{\rm abs} j_{\rm ph}$, where $N_{\rm low}$ is the number of atoms in the state that is absorbing the photon flux $j_{\rm ph}$. Correspondingly, the number of stimulated emissions per unit time is $N_{\rm em} = N_{\rm up} B_{\rm em} j_{\rm ph}$, where $N_{\rm up}$ is the number of atoms in the upper state and $B_{\rm em}$ is the Einstein coefficient of stimulated emission. These relations are at the heart of the XFEL interaction with matter and are explicitly used in most laser–matter simulations.[18–24]

However, technological progress in the generation of ultrashort XFEL pulses with durations of the order of a few tens of attoseconds,[25–27] the "fine structure" of self-amplified spontaneous-emission (SASE) pulses[25,28–31] (spike durations of the order of 0.1–0.2 fs), and high-harmonic generation (HHG) with durations down to 67 as[32] raise questions about the applicability of the basic quantum mechanical framework of a constant probability per unit of time. In fact, the standard probability per unit time w corresponds to pulse durations long enough to be approximated by a single mode of radiation with constant w. An ultrashort pulse, however, is composed of different spectral components, each of which corresponds to a different w value (in an envelope of modes) with typical frequency width of the order of $1/\tau$. In this case, the total probability is determined by the sum of specific w values, which is not proportional to the duration τ.

To develop a physically transparent description, let us consider ultrashort pulse theory in the framework of Fermi's equivalent-photon concept.[33] An ultrashort pulse can then be represented as a composition of monochromatic modes (equivalent photons) with amplitudes equal to the Fourier pulse transformation. After multiplication of a specific mode by the cross-section of the elementary atomic process and summation over all frequencies in the pulse, we arrive at the following expression for the total probability:[34]

$$W(\omega_c, \tau) = \frac{c}{4\pi^2}\int_0^{+\infty} \sigma_{\rm abs}(\omega)\frac{|E(\omega, \omega_c, \tau)|^2}{\hbar\omega}\, d\omega, \quad (3)$$

where c is the speed of light, ω_c is the carrier frequency, $E(\omega)$ is the Fourier transform of the electric field strength of the incident pulse, and $\sigma_{\rm abs}$ is the usual absorption cross-section. According to the optical theorem and in the framework of the dipole approximation, the absorption cross-section spectrum can be expressed through the dynamical polarizability α:[35]

$$\sigma_{\rm abs}(\omega) = \frac{4\pi\omega}{c}\,{\rm Im}\,\alpha(\omega). \quad (4)$$

In turn, the dynamical polarizability (in atomic units) can be calculated using the real $[f_1(\omega)]$ and imaginary $[f_2(\omega)]$ parts of the atomic scattering factor:[36]

$$\alpha(\omega) = \frac{f_1(\omega) + i\cdot f_2(\omega)}{\omega^2}, \quad (5)$$

and finally the absorption cross-section spectrum can be expressed via the imaginary part of the scattering factor, which is tabulated over a wide range of energies and elements:[37]

$$\sigma_{\rm abs}(\omega) = \frac{4\pi}{c\omega} f_2(\omega). \quad (6)$$

The importance of the nonlinearity in the photoionization process can best be demonstrated analytically by employing Kramers' formula for the photoionization,

$$\sigma_n(\omega) \approx \frac{8\pi}{3^{3/2}}\frac{Z_{\rm eff}^4}{cn^5\omega^3}, \quad (7)$$

and the squared modulus of the Fourier component of a corrected Gaussian pulse shape,[38]

$$|E(\omega, \omega_c, \tau)|^2 \approx \frac{\pi}{2}E_0^2\tau^2\frac{\omega^2\tau^2}{1+\omega_c^2\tau^2}\exp\left[-(\omega_c-\omega)^2\tau^2\right], \quad (8)$$

where n is the principal quantum number, $Z_{\rm eff}$ is the effective charge of the ion core, E_0 is the electric field amplitude, ω and ω_c are the current and carrier frequencies, and τ is the pulse duration. Kramers' formula has a high precision even for the ground state of H-like ions[39] and allows one to consider any quantum state n (whereas the exact Sommerfeld formula is only applicable to the H-like ground state $1s^2S_{1/2}$). Inserting Eqs. (7) and (8) into Eq. (3), we obtain

$$W_n \approx \frac{4\pi^{1/2}}{3^{3/2}}\frac{E_0^2}{E_n^2}\frac{\tilde\tau^5}{1+\tilde\tau^2\tilde\omega^2}\,{\rm erfc}\left[\tilde\tau(1-\tilde\omega)\right], \quad (9)$$

where $\tilde\tau = \tau I_n$, $\tilde\omega = \omega_c/I_n$, $I_n = Z_{\rm eff}^2/2n^2$, $E_n = Z_{\rm eff}^3/2n^{5/2}$, and erfc is the complementary error function. We can see from Eq. (9) that the ionization probability depends in a highly nonlinear manner on frequency and pulse duration. In the long-pulse limit, if $\tilde\omega < 1$, we obtain $W_n(\tilde\tau \gg 1) \rightarrow 0$, whereas in the opposite case when $\tilde\omega > 1$, we find $W_n(\tilde\tau \gg 1) \propto \tilde\tau$.

Handling the random nature of the SASE spikes is difficult for both theory and experiment. For example, the necessary data normalization of absorption measurements for random pulses is quite

challenging: either a very large number of pulses have to be accumulated,[40] which is very inconvenient for samples heated with optical lasers, where timing issues are important, or a twofold normalization procedure has to be applied[5] to find a compromise between persistent random features and typically low shot numbers (5–20; see, e.g., Ref. 5) for warm dense matter samples. From a theoretical point of view, random parameters in simulations are challenging, since the differentiation of general or specific features in the XFEL–matter interaction is not a trivial task.

To obtain insight into the general features driven by random pulses, we represent an XFEL pulse with carrier frequency ω_c as a series of n modulated Gaussian spikes with envelopes of Gaussian shape:

$$E(t) = E_0 \sum_{j=1}^{n} \exp\left(-\frac{t_j^2}{2T^2}\right)\exp\left[-\frac{(t-t_j)^2}{2\tau^2}\right]\cos\left[\omega_c(t-t_j)+\varphi_j\right], \tag{10}$$

where t_j and φ_j are the time of maximum and the initial phase of the jth pulse. The characteristic durations of a single spike and envelope are denoted by τ and T, respectively. Here and throughout the following, we consider E_0 to be equal to 1 a.u. If it is assumed that the spikes do not overlap with each other, then the Fourier transform of the pulse train according to Eq. (10) is given by

$$E(\omega) = \sqrt{\frac{\pi}{2}}E_0\tau\sum_{j=1}^{n}\exp\left(-\frac{t_j^2}{2T^2}+i\omega t_j\right)\left\{\exp\left[-i\varphi_j-\frac{(\omega-\omega_c)^2\tau^2}{2}\right]\right.$$
$$\left.+\exp\left[i\varphi_j-\frac{(\omega+\omega_c)^2\tau^2}{2}\right]\right\}, \tag{11}$$

while the time at maximum of the jth regular spike is given by

$$t_j^0 = \frac{\varkappa T}{2}\left(\frac{2j-1}{n}-1\right), \quad j=1,\ldots,n, \quad n<\left\lfloor\frac{T}{\tau}\right\rfloor. \tag{12}$$

It should be noted that the approximate time duration of the envelope is $\varkappa T$, where $\varkappa \approx 6$–8. The model indicates that the initial phases of regular spikes are equal to zero and that the corresponding t_j parameters are equal to t_j^0. In the case of random spikes, the phases φ_j are distributed uniformly over the interval $[-\pi,\pi]$, while the parameters t_j are uniformly distributed over the intervals $[t_j^0-\Delta_t, t_j^0+\Delta_t]$. Δ_t satisfies the following constraint related to the overlap of spikes:

$$\Delta_t = \frac{\varkappa}{2}\left(\frac{T}{n}-\tau\right). \tag{13}$$

Since we seek to apply the signal model also with random parameters to the description of the ionization process, it is necessary to obtain the expectation value $M\left[|E(\omega)|^2\right]$ of the squared modulus of the Fourier transform:

$$M\left[|E(\omega)|^2\right] = \frac{\pi^{3/2}\tau^2 T}{8\Delta_t}\left\{\exp\left[-(\omega-\omega_c)^2\tau^2\right]\right.$$
$$\left.+\exp\left[-(\omega+\omega_c)^2\tau^2\right]\right\}$$
$$\times\sum_{j=1}^{n}\left[\operatorname{erf}\left(\frac{t_j^0+\Delta_t}{T}\right)-\operatorname{erf}\left(\frac{t_j^0-\Delta_t}{T}\right)\right], \tag{14}$$

$$\varepsilon_{\text{tot}} = \int_{-\infty}^{+\infty}E^2(t)\,dt$$
$$= \frac{\sqrt{\pi}}{2}E_0^2\tau\sum_{j=1}^{n}\sum_{k=1}^{n}\exp\left[-\frac{t_j^2+t_k^2}{2T^2}-\frac{(t_j-t_k)^2}{4\tau^2}\right]$$
$$\times\left\{\exp(-\omega_c^2\tau^2)\cos(\varphi_j+\varphi_k)\right.$$
$$\left.+\cos\left[\omega_c(t_j-t_k)-(\varphi_j-\varphi_k)\right]\right\}, \tag{15}$$

where ε_{tot} is the power spectral density. We have obtained the expectation formula for the squared modulus of the spectral density under the assumption that the probability densities $p(t_j)$ and $p(\varphi_j)$ are constant and equal to $1/2\Delta_t$ and $1/2\pi$, respectively (for more details, see the Appendix).

The spectrum of regular/random spikes and the expectation values are shown in Fig. 1. Here and in the following figures, values are divided by the total signal energy $\varepsilon_{\text{tot}} = \int_{-\infty}^{+\infty}E^2(t)\,dt$ [in order to remove the trivial dependence on total energy related to pulse duration; see the discussion below of Eq. (16)]. The curve of the expectation value has a Gaussian shape. The magnitude of the regular spikes is approximately two times larger because in this case all pulse energy is concentrated into narrow spectral lines.

A random partial-coherence approach was employed in Ref. 41 to calculate a set of pulse shapes and numerically retrieve the characteristics measured at the FLASH FEL.[42] The approach adopted in this article is different in that it identifies common features in any XFEL pulse shape and hence is more generalized.

Let us now study the impact of spikes within a laser pulse on the ionization probability. Figure 2 shows the ionization probability W of solid aluminum for different carrier frequencies. For better demonstration, the probability W is divided by the power spectral density of the pulse ε_{tot} [see Eq. (15)]. The curves demonstrate that for all carrier frequencies (above or below threshold), the dependence of the

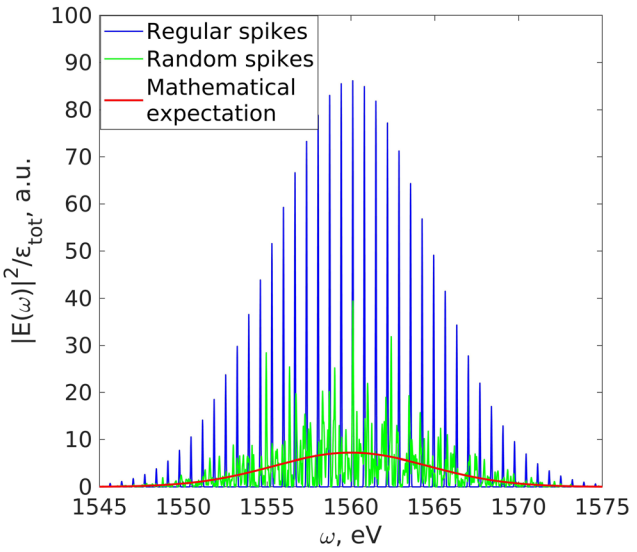

FIG. 1. Spectrum of the squared modulus of the pulse Fourier transform divided by the total signal energy ϵ_{tot}; see the text. The blue, green, and red curves represent the calculations for regular spikes, the simulations for random spikes, and the expectation values, respectively. The parameters of the pulse are $T = 20$ fs, $\tau = 0.1$ fs, $\omega_c = 1560$ eV, and $n = 20$.

total probability $W(\tau)/\varepsilon_{\rm tot}(\tau)$ on the spike duration τ is not constant: the nonlinear behavior is qualitatively equivalent to the single-pulse effects discussed in relation to Eqs. (7)–(9) and distinctly different from the standard theory of photoionization. The nonmonotonic behavior is very pronounced for $\tau \le 0.2$ fs. This nonlinear behavior manifests itself in $W(\tau)/\varepsilon_{\rm tot}(\tau) \neq$ const and is of particular practical importance, since typical spike durations in XFEL SASE pulses are of the order of 0.1–0.2 fs.[25,28–31]

Let us now explore the physical origin of the nonlinear dependences. The standard long-pulse behavior, namely,

$$\frac{W(\omega,\tau)}{\varepsilon_{\rm tot}} = \frac{c\sigma_{\rm abs}(\omega)}{4\pi\omega}, \tag{16}$$

is obtained from Eq. (3) in the long-pulse limit and for carrier frequencies that are larger than the ionization threshold: this corresponds to Fermi's golden rule of constant probability per unit time. Figure 2 shows that for carrier frequencies lower than the ionization threshold, the dependence of $W(\tau)/\varepsilon_{\rm tot}(\tau)$ is not constant and tends to zero for increasing spike duration (see the curves for $\omega_c = 1559$ eV and $\omega_c = 1555$ eV). At some limiting values of τ, the signal band becomes too narrow such that all spectral components in Eq. (11) are lower than the ionization threshold. At carrier frequencies higher than the ionization threshold (see the curves for $\omega_c = 1565$, 1570, and 1575 eV), the monotonically increasing values of $W(\tau)/\varepsilon_{\rm tot}(\tau)$ for increasing spike duration τ are due to the narrowing of the signal band: the long-pulse limit is continuously approached for each single spike, and all spectral components are located in the vicinity of the carrier frequency. At large spike durations, all the signal band is above the ionization threshold, and the $W(\tau)/\varepsilon_{\rm tot}(\tau)$ dependence saturates. This is the regime where Eq. (16) applies.

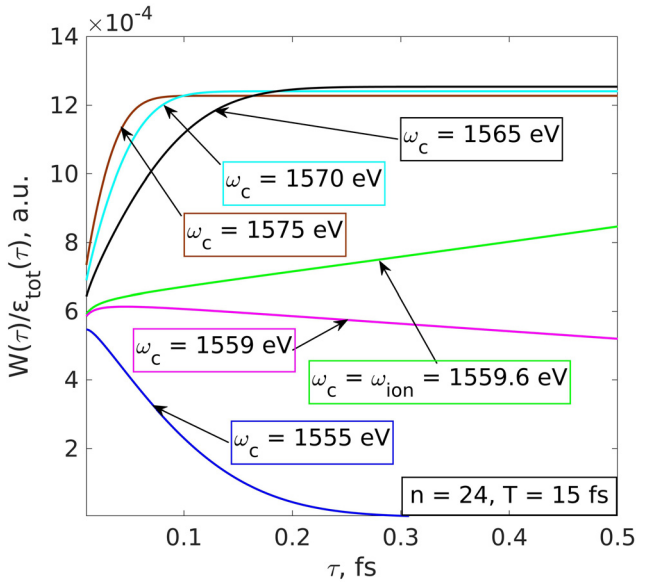

FIG. 2. Total probability of *K*-shell ionization of solid aluminum for different carrier frequencies ω_c as a function of the pulse duration τ of a single spike. Spikes are equidistant with zero phase, the envelope characteristic time $T = 15$ fs, and the number of spikes $n = 24$. The *K*-shell ionization threshold is at $\hbar\omega_{\rm ion} = 1559.6$ eV.

To demonstrate the principal effects of the short-pulse theory of the inner-shell electron ionization process of warm dense matter outlined above, we develop a simple but finite-temperature absorption model. Taking into account the Fermi distribution for the cross-section spectrum calculation at arbitrary temperature, we obtain

$$\sigma_{\rm abs}(\omega,\Theta) \approx C_1 + \frac{4\pi}{c\omega} C_2 F(\Theta), \tag{17}$$

with

$$F(\Theta) = 1 - \frac{1}{\exp\left[\left(\hbar\omega - \hbar\omega_{\rm ion} + \Theta_f - \mu(\Theta)\right)/\Theta\right] + 1}, \tag{18}$$

where Θ is the electron temperature in eV. Equations (17) and (18) are applied to the ionization of the *K* shell of solid aluminum, with the *K*-shell ionization energy taken as $\hbar\omega_{\rm ion} = 1559.6$ eV[43] and the Fermi temperature taken as $\Theta_f = 11.7$ eV.[44] The coefficients C_1 and C_2 are calculated according to data on the spectral cross-section at room temperature and employing Eq. (6) and the imaginary part of the atomic form factor as given in Ref. 37: $C_1 = 7.4 \times^{-4}$ a.u. and $C_2 = 3.8$ a.u. Finally, the chemical potential $\mu(\Theta)$ is evaluated numerically[45] for the electron density in the conduction band of solid aluminum ($n_e = 1.8 \times 10^{23}$ cm^{-3}).

Figure 3 shows the spectral *K*-shell absorption cross-section of solid aluminum for different temperatures. It can clearly be seen that the absorption edge becomes smoother with increasing temperature. We note that the slope of the absorption cross-section can be employed as a temperature diagnostic in warm dense matter.[6]

Let us now apply the simple finite-temperature *K*-shell absorption model of aluminum to demonstrate the principal effects on the ionization probability induced by x-ray pulses consisting of spikes. Figure 4 displays the calculated results for the ionization probability as a function of the carrier frequency ω_c for regular spikes with different single-spike durations. When the carrier frequency is below the ionization threshold, short-pulse spikes effectively change the apparent slope of the spectral

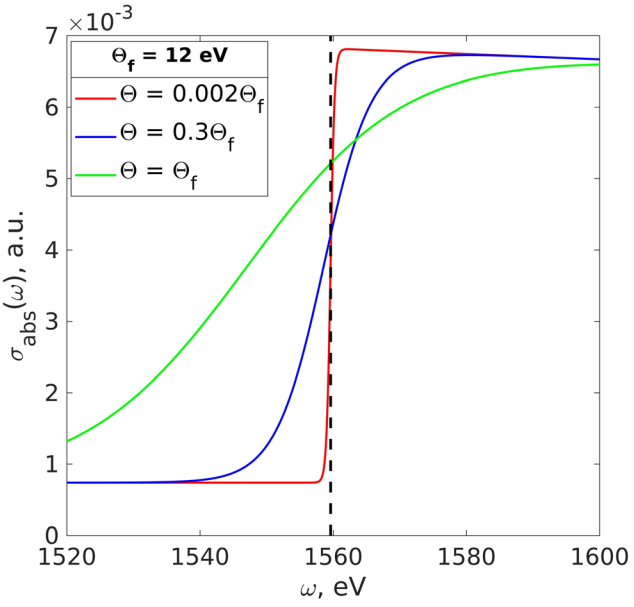

FIG. 3. Energy dependence of the *K*-shell absorption cross-section of solid aluminum for different temperatures near threshold.

absorption probability $W(\omega_c)/\varepsilon_{tot}(\omega_c)$: the shorter the pulse duration of the spikes, the flatter is the absorption probability. The pronounced probabilities below threshold for short pulses are due to the broadening of the Fourier transform of the total spectral pulse, which provides spectral components exceeding the ionization threshold.

To evaluate the relative importance of temperature and ultrashort pulses, Fig. 5 shows the spectral absorption probability for a single Gaussian pulse and an x-ray pulse consisting of regular spikes. For example, the relative impact of temperature and short-pulse effects can be obtained by comparing the ionization probability (divided by ϵ_{tot}) for a single Gaussian pulse with a pulse duration $\tau_G = 20$ fs at temperature $\Theta = 2.4$ eV with that for an x-ray pulse containing spikes with the same envelope duration $T = 20$ fs and typical spike duration $\tau = 0.1$ fs but at room temperature $\Theta = 0.025$ eV. The effects of temperature and of ultrashort pulses are similar in this example, since the respective curves have a similar appearance.

We now explore the general features of photoionization driven by different types of spikes. Figure 6 explores the ionization probability as a function of the carrier frequency ω_c in the case of random spikes. The curves show results for two different spike pulse durations $\tau = 0.1$ and 0.05 fs. The envelope parameters are $T = 20$ fs and $n = 50$ spikes, and the temperature is room temperature $\Theta = 0.025$ eV. The solid lines are the simulations for random spikes (with different colors indicating different simulations, i.e., different random parameters), the dashed lines are the simulations for the corresponding regular spikes (discussed in relation to Fig. 1) and the crosses are the simulations for the expectation values [Eqs. (14) and (15)]. It is observed that the absorption cross-section profile at finite temperature becomes smoother with decreasing regular spike duration, and the same tendency also holds for the random spikes in Fig. 6. It is likewise observed that the results of the expectation value approach are in very good agreement with those of the numerical calculations.

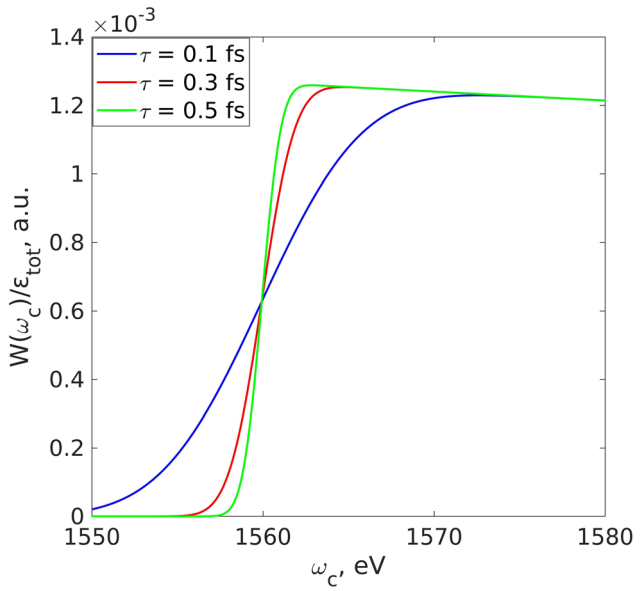

FIG. 4. Ionization probability of *K*-shell absorption in solid aluminum as a function of carrier frequency for different durations of regular spikes for $T = 20$ fs, $n = 20$, and $\Theta = 0.025$ eV.

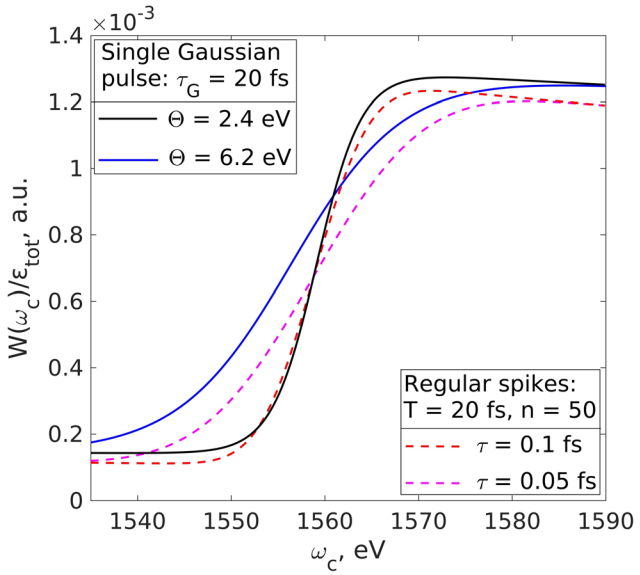

FIG. 5. Ionization probability as a function of carrier frequency. Solid lines correspond to single Gaussian pulses of duration $\tau_G = 20$ fs at different temperatures $\Theta = 2.4$ eV (black) and 6.2 eV (blue). Dot-dashed lines correspond to x-ray pulses composed of regular spikes at room temperature for $T = 20$ fs, $n = 50$, and spike duration $\tau = 0.1$ fs (red) and 0.05 fs (magenta).

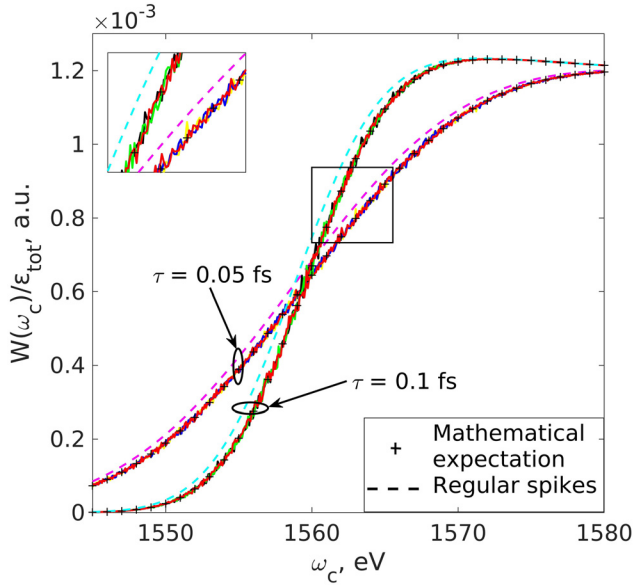

FIG. 6. Probability of *K*-shell ionization of solid aluminum as a function of carrier frequency for $T = 20$ fs, $n = 50$, $\Theta = 0.025$ eV, and different durations of random spikes. Solid lines are simulations for random spikes (with different colors corresponding to different runs of random parameters), dashed lines are simulations for regular spikes, and crosses represent the results of the expectation value approach.

Moreover, the simulations demonstrate that the differences between the ionization probabilities for random and regular spikes are rather small (the fact that the absolute values for regular spikes are slightly lower is a particular case and is related to the simultaneous features of equidistant spikes and zero phases). Therefore, random simulations and the expectation value approach are useful approximations for any cases of interest, i.e., cases that are neither totally regular nor totally random. This is of great practical importance, since there is usually only limited knowledge of random and regular parameters in experiments.

In summary, we have generalized photoionization theory to ultrashort x-ray pulses, where the standard approach of constant probability per unit time (Fermi's golden rule together with Einstein's theory of stimulated emission and absorption) does not apply. A model has been developed where an XFEL pulse is represented by an envelope with a carrier frequency and a series of spikes for two different regimes: (i) spikes with random initial phases and random times for spike maxima and (ii) regular spikes. An analytical model of finite-temperature dense matter using the Fermi distribution has allowed us to explore the effects of ultrashort pulses on dense matter under extreme conditions. In the vicinity of the ionization threshold, the dependence of the ionization probability on carrier frequency rises from zero to a constant value for solid matter at room temperature. By contrast, calculations for a single Gaussian pulse with a duration equal to the XFEL pulse envelope recover the standard dependence in the form of a sharp step function. Simulations for typical target and laser parameters have revealed general properties for x-ray pulses containing spikes (e.g., XFEL SASE pulses): the dependences of the nonlinear photoionization probability on carrier frequency and spike duration for random spikes and regular spikes are very similar, indicating that the model developed here can be applied to a wide variety of practical cases even if random and regular contributions are not well known (as is typical in experiments). As almost all x-ray pulse–matter interactions proceed from photoabsorption, the generalized ultrashort pulse model and the analytical expectation value approach are of interest for a wide variety of simulations of the interaction of XFEL beams with matter.

ACKNOWLEDGMENT

This work was funded by RFBR Grant No. 19-32-90016, Ecole Polytechnique, the Cooperation Agreement between the Sorbonne University and MIPT, and the MIPT 5-top-100 program. This work has also been supported by the Competitiveness Program of NRNU MEPhI in the framework of the Russian Academic Excellence Project.

APPENDIX: EXPECTATION VALUE APPROACH

Using Eq. (3) and the linearity of M, we obtain

$$M[W] = M\left[\frac{c}{4\pi^2}\int_0^{+\infty}\sigma_{\mathrm{abs}}(\omega)\frac{|E(\omega,\omega_c,\tau)|^2}{\hbar\omega}d\omega\right] = \frac{c}{4\pi^2}\int_0^{+\infty}\frac{\sigma_{\mathrm{abs}}(\omega)}{\hbar\omega}M\left[|E(\omega)|^2\right]d\omega. \quad \text{(A1)}$$

To simplify this equation further, we define the following variables for the Fourier transform [see Eq. (11)]:

$$X_j = \sqrt{\frac{\pi}{2}}E_0\tau\sum_{j=1}^{n}\exp\left(-\frac{t_j^2}{2T^2}+i\omega t_j\right), \quad \text{(A2)}$$

$$Y_j = \exp\left[-i\varphi_j-\frac{(\omega-\omega_c)^2\tau^2}{2}\right]+\exp\left[i\varphi_j-\frac{(\omega+\omega_c)^2\tau^2}{2}\right]. \quad \text{(A3)}$$

As spikes are not correlated with each other, $\{X_j\}_{j=1}^n$ and $\{Y_j\}_{j=1}^n$ together comprise a set of $2n$ independent random functions. The formula for the squared modulus of the spectral density expectation can then be rewritten as

$$M\left[|E(\omega)|^2\right] = M\left[\sum_{j=1}^{n}X_jY_j\sum_{k=1}^{n}X_k^*Y_k^*\right] = \sum_{j=1}^{n}\sum_{k=1}^{n}M[X_jX_k^*]M[Y_jY_k^*]. \quad \text{(A4)}$$

If $k\neq j$, then $M[Y_jY_k^*] = M[Y_j]M[Y_k^*]$. As we assume that t_j and ϕ_j are distributed uniformly, the probability densities $p(t_j)$ and $p(\varphi_j)$ are constant and equal to $1/2\Delta_t$ and $1/2\pi$, respectively:

$$M[Y_j] = \int_{-\infty}^{+\infty}Y_jp(\varphi_j) = \frac{1}{2\pi}\exp\left[-\frac{(\omega+\omega_c)^2\tau^2}{2}\right]\int_{-\pi}^{+\pi}\exp(-\varphi_j)\,d\varphi_j + \frac{1}{2\pi}\exp\left[-\frac{(\omega+\omega_c)^2\tau^2}{2}\right]\int_{-\pi}^{+\pi}\exp(\varphi_j)\,d\varphi_j = 0. \quad \text{(A5)}$$

Because $M[Y_j] = 0$, Eq. (A4) can be transformed to

$$M\left[|E(\omega)|^2\right] = \sum_{j=1}^{n}\sum_{k=1}^{n}M[X_jX_k^*]M[Y_jY_k^*]\delta_{jk} = \sum_{j=1}^{n}M\left[|X_j|^2\right]M\left[|Y_j|^2\right]. \quad \text{(A6)}$$

The next step is to calculate the mathematical expectations $|X_j|^2$ and $|Y_j|^2$ and then substitute the result into Eq. (A6). We thereby obtain the expectations for the Fourier transforms:

$$M\left[|X_j|^2\right] = \int_{-\infty}^{+\infty}|X_j|^2p(t_j)\,dt_j = \frac{\pi E_0^2\tau^2}{4\Delta_t}\int_{t_j^0-\Delta_t}^{t_j^0+\Delta_t}\exp\left(-\frac{t_j^2}{T^2}\right)dt_j = \frac{\pi^{3/2}E_0^2\tau^2T}{8\Delta_t}\left[\mathrm{erf}\left(\frac{t_j^0+\Delta_t}{T}\right)-\mathrm{erf}\left(\frac{t_j^0-\Delta_t}{T}\right)\right], \quad \text{(A7)}$$

$$M\left[|Y_j|^2\right] = \int_{-\infty}^{+\infty}|Y_j|^2p(\varphi_j)d\varphi_j = \frac{1}{2\pi}\int_{-\pi}^{\pi}\left\{\exp\left[-(\omega-\omega_c)^2\tau^2\right]+\exp\left[-(\omega+\omega_c)^2\tau^2\right] + 2\exp\left[-(\omega^2+\omega_c^2)\tau^2\right]\cos(2\varphi_j)\right\}d\varphi_j = \exp\left[-(\omega-\omega_c)^2\tau^2\right]+\exp\left[-(\omega+\omega_c)^2\tau^2\right], \quad \text{(A8)}$$

$$M\left[|E(\omega)|^2\right] = \frac{\pi^{3/2}E_0^2\tau^2T}{8\Delta_t}\left\{\exp\left[-(\omega-\omega_c)^2\tau^2\right]+\exp\left[-(\omega+\omega_c)^2\tau^2\right]\right\} \times\sum_{j=1}^{n}\left[\mathrm{erf}\left(\frac{t_j^0+\Delta_t}{T}\right)-\mathrm{erf}\left(\frac{t_j^0-\Delta_t}{T}\right)\right]. \quad \text{(A9)}$$

On substituting Eq. (A9) into Eq. (A1), we can numerically calculate the expectation value for the ionization probability.

REFERENCES

[1]W.-D. Kraeft, D. Kremp, W. Ebeling, and G. Röpke, *Quantum Statistics of Charged Particle Systems* (Akademie-Verlag, Berlin, 1986).
[2]S. Ichimaru, *Statistical Plasmas Physics Vol. II: Condensed Plasmas* (Westview Press, Oxford, 2004).
[3]R. Drake, *High-Energy-Density Physics* (Springer, Berlin, 2006).
[4]F. Graziani, M. P. Desjarlais, R. Redmer, and S. B. Trickey, *Frontiers and Challenges in Warm Dense Matter* (Springer Science & Business, 2014), Vol. 96.
[5]M. Harmand, A. Ravasio, S. Mazevet *et al.*, "X-ray absorption spectroscopy of iron at multimegabar pressures in laser shock experiments," Phys. Rev. B **92**, 024108 (2015).
[6]F. Dorchies, F. Festa, V. Recoules *et al.*, "X-ray absorption *K*-edge as a diagnostic of the electronic temperature in warm dense aluminum," Phys. Rev. B **92**, 085117 (2015).
[7]S. Zhang, S. Zhao, W. Kang *et al.*, "Link between *K* absorption edges and thermodynamic properties of warm dense plasmas established by an imporved first-principles method," Phys. Rev. B **93**, 115114 (2016).
[8]R. Cheng, Y. Lei, X. Zhou *et al.*, "Warm dense matter research at HIAF," Matter Radiat. Extremes **3**, 85 (2018).
[9]R. W. Lee, S. J. Moon, H.-K. Chung *et al.*, "Finite temperature dense matter studies on next generation light sources," J. Opt. Soc. Am. B **20**, 770 (2003).
[10]D. Riley, "Generation and characterisation of warm dense matter with intense lasers," Plasma Phys. Controlled Fusion **60**, 014033 (2017).
[11]O. Renner, M. Šmíd, D. Batani, and L. Antonelli, "Suprathermal electron production in laser-irradiated Cu targets characterized by combined methods of x-ray imaging and spectroscopy," Plasma Phys. Controlled Fusion **58**, 075007 (2016).
[12]O. Renner and F. B. Rosmej, "Challenges of x-ray spectroscopy in investigations of matter under extreme conditions," Matter Radiat. Extremes **4**, 024201 (2019).
[13]M. Smid, O. Renner, A. Colaitis *et al.*, "Characterization of suprathermal electrons inside laser accelerated solid density matter via axially-resolved K_α-emission," Nat. Commun. **10**, 4212 (2019).
[14]*Free Electron Lasers*, edited by S. Varro (Intech, Rijeka, 2012).
[15]https://lcls.slac.stanford.edu, X-ray FEL LCLS, 2020.
[16]https://www.xfel.eu/, X-ray FEL EU-XFEL, 2020.
[17]http://xfel.riken.jp/eng/, X-ray FEL SACLA, 2020.
[18]O. Gorobtsov, U. Lorenz, N. Kabachnik *et al.*, "Theoretical study of electronic damage in single-particle imaging experiments at x-ray free-electron lasers for pulse durations from 0.1 to 10 fs," Phys. Rev. E **91**, 062712 (2015).
[19]A. G. de la Varga, P. Velarde, F. de Gaufridy *et al.*, "Non-Maxwellian electron distributions in time-dependent simulations of low-*Z* materials illuminated by a high-intensity X-ray laser," High Energy Density Phys. **9**, 542 (2013).
[20]S. J. Rose, "The effect of a radiation field on exciation and ionisation in non-LTE high energy density plasmas," High Energy Density Phys. **5**, 23 (2009).
[21]H.-K. Chung, M. H. Chen, W. L. Morgan *et al.*, "FLYCHK: Generalized population kinetics and spectral model for rapid spectroscopic analysis for all elements," High Energy Density Phys. **1**, 3 (2005).
[22]C. Gao, J. Zeng, and J. Yuan, "Evolution dynamics of charge state distribution in neon interaction with x-ray pulses of variant intensities and durations," High Energy Density Phys. **14**, 52 (2015).
[23]S.-K. Son, L. Young, and R. Santra, "Impact of hollow-atom formation on coherent x-ray scattering at high intensity," Phys. Rev. A **83**, 033402 (2011).
[24]O. Peyrusse, "Coupling of detailed configuration kinetics and hydrodynamics in materials submitted to x-ray free-electron-laser radiation," Phys. Rev. E **86**, 036403 (2012).
[25]E. Schneidmiller and M. Yurkov, "Photon beam properties at the European XFEL," Technical Report No. XFEL.EU TR-2011-006, Deutsches Elektronen-Synchrotron DESY, 2011.
[26]T. Tanaka, "Proposal to generate an isolated monocycle x-ray pulse by counteracting the slippage effect in free-electron lasers," Phys. Rev. Lett. **114**, 044801 (2015).
[27]Y. Kida, R. Kinjo, and T. Tanaka, "Synthesizing high-order harmonics to generate a sub-cycle pulse in free-electron lasers," Appl. Phys. Lett. **109**, 151107 (2016).
[28]G. Geloni, E. Saldin, L. Samoylova *et al.*, "Coherence properties of the European XFEL," New J. Phys. **12**, 035021 (2010).
[29]S. Roling, H. Zacharias, L. Samoylova *et al.*, "Time-dependent wave front propagation simulation of a hard x-ray split-and-delay unit: Towards a measurement of the temporal coherence properties of x-ray free electron lasers," Phys. Rev. Spec. Top.–Accel. Beams **17**, 110705 (2014).
[30]B. Li, "X-ray photon temporal diagnostics for the European XFEL," Technical Report No. XFEL.EU TN-2012-002-01, Deutsches Elektronen-Synchrotron DESY, 2012.
[31]Z. Huang and K.-J. Kim, "Review of x-ray free-electron laser theory," Phys. Rev. Spec. Top.–Accel. Beams **10**, 034801 (2007).
[32]K. Zhao, Q. Zhang, M. Chini *et al.*, "Tailoring a 67 attosecond pulse through advantageous phase-mismatch," Opt. Lett. **37**, 3891 (2012).
[33]E. Fermi, "Über die theorie des stosses zwischen atomen und elektrisch geladenen teilchen," Z. Phys. **29**, 35 (1924).
[34]V. A. Astapenko, 'Simple formula for photoprocesses in ultrashort electromagnetic field," Phys. Lett. A, **374**, 1585 (2010); F. B. Rosmej, V. A. Astapenko, and V. S. Lisitsa, "Generalized scaling laws for ionization of atomic states by ultra-short electromagnetic pulses," J. Phys. B: At., Mol. Opt. Phys. **49**, 025602 (2016).
[35]R. G. Newton, "Optical theorem and beyond," Am. J. Phys. **44**, 639–642 (1976).
[36]F. B. Rosmej, V. A. Astapenko, and V. S. Lisitsa, "XUV and x-ray elastic scattering of attosecond electromagnetic pulses on atoms," J. Phys. B: At., Mol. Opt. Phys. **50**, 235601 (2017).
[37]B. L. Henke, E. M. Gullikson, and J. C. Davis, "X-ray interactions: Photoabsorption, scattering, transmission, and reflection at $E = 50$-30, 000 eV, $Z = 1$-92," At. Data Nucl. Data Tables **54**, 181–342 (1993).
[38]Q. Lin, J. Zheng, and W. Becker, "Subcycle pulsed focused vector beams," Phys. Rev. Lett. **97**, 253902 (2006).
[39]F. B. Rosmej, L. A. Vainshtein, V. A. Astapenko, and V. S. Lisitsa, "Statistical and quantum photoionization cross sections in plasmas: Analytical approaches for any configurations including inner shells," Matter Radiat. Extremes **5**, 064202 (2020).
[40]T. Katayama, Y. Inubushi, Y. Obara *et al.*, "Femtosecond x-ray absorption spectroscopy with hard x-ray free electron laser," Appl. Phys. Lett. **103**, 131105 (2013).
[41]T. Pfeifer, Y. Jiang, S. Düsterer *et al.*, "Partial-coherence method to model experimental free-electron laser pulse statistics," Opt. Lett. **35**, 3441 (2010).
[42]https://flash.desy.de/, XUV-FEL FLASH, 2020.
[43]A. Thompson, D. Attwood, E. Gullikson *et al.*, *X-Ray Data Booklet* (Lawrence Berkely National Laboratory, University of California, 2009).
[44]N. Ashcroft and N. Mermin, *Solid State Physics* (Holt-Saunders, Philadelphia, 1976), p. 16.
[45]F. B. Rosmej, V. S. Lisitsa, and V. A. Astapenko, *Plasma Atomic Physics*, Springer Series on Atomic, Optical and Plasma Physics (Springer, Heidelberg, 2021).